International Journal of Hospital Research 2020, 9(2)
http://ijhr.iums.ac.ir
Research Article

The Diagnosis of Patients Suspected to Bone Marrow Metastasis based on Multivariate Control Chart

Mahmood Shahrabi[1], Amirhossein Amiri[2*], Hamidreza Saligheh Rad[3], Sedigheh Ghofrani[4]

[1]Department of Industrial Engineering, South Tehran Branch, Islamic Azad University, Tehran, Iran
[2]Department of Industrial Engineering, Faculty of Engineering, Shahed University, Tehran, Iran.
[3] Department of Medical Physics and Biomedical Engineering, Tehran University of Medical Sciences, Tehran, Iran
[4]Department of Electrical and Electronic Engineering, South Tehran Branch, Islamic Azad University, Tehran, Iran

Abstract

Background and Objectives: One of the currently important and widely used research subjects in the healthcare area of cancer patients is the diagnosis procedure of cancer tumors and metastases in magnetic resonance imaging such that it has a high level of accuracy and also be a support for doctors in interpreting and diagnosing medical data. To this aim, a multivariate Hotelling's T^2 control chart is used.
Methods: Using a two-dimensional discrete wavelet transform, some features of the image texture are extracted by using statistical and transform methods. Then, to reduce the data dimensions and feature selection, a genetic algorithm is used. Afterward, two methods including fuzzy c-Means clustering algorithm and a multivariate Hotelling's T^2 control chart are used to diagnose bone marrow metastasis patients.
Results: From 204 bone marrow samples, 76 features are extracted from which six ones are selected and a 204×6 feature vector matrix is generated. Finally, the performance of the proposed two methods is compared. The results show that the diagnosis and accuracy measures of multivariate Hotelling's T^2 control chart are better than the other method.
Conclusions: In the context of cancer, one of the current concerns for healthcare providers is to use non-invasive, short response time, and highly accurate methods in diagnosing tumors and metastases. The proposed method appropriately addresses these requirements.

Keywords: Bone marrow metastases, Multivariate Hotelling's T^2 control chart, Fuzzy clustering, Feature extraction.

Background and Objectives

Bone marrow constitutes the inner part of the bone and plays a key role in producing and forming blood cells[1,2]. Since there is a greater flow of blood in this area in comparison to the cortical layer of bone, main factor in the formation of metastases in bone and bone marrow areas. Red bone marrow exists in the axial skeleton including vertebrae, pelvis region, femur, skull, and ribs, and due to the cancer cells transferred to these regions through the bloodstream, there is more probability of emergence of metastases in these regions[1]. Many studies have been conducted on the timely diagnosis of cancer tumors and metastases. However, the method which is usually used for final diagnosis is the pathological examination. This method, in spite of its capabilities in diagnosing a variety of diseases, suffers from problems such as invasively (the need for sampling), relatively long response time and results that depend on the experience and expertise of the pathologist[3]. Therefore, different techniques have been proposed in the past years to solve these problems. Among which, magnetic resonance imaging (MRI) methods, which can be employed in a non-invasive and non-destructive way for producing multi-spectral images, have received considerable interest.To produce MRI images, electromagnetic waves are used.

*Corresponding Author: Amirhossein Amiri2
Email: amiri@shahed.ac.ir

The electromagnetic waves used for imaging are in the frequency range of radio waves which are transformed to the image using the Fourier transform. This image is very precise so that very small changes can be detected[4]. Due to the complexity of body tissues, manual diagnosis of pelvic region tissues and metastases are extremely time-consuming and depend on the operator's conditions. Moreover, the vital need for experts who analyze the images and diagnose the problems makes the ordinary and traditional methods inefficient in the absence of experts. Thus, for accurate examination of metastases, computer-aided medical images processing techniques and algorithms can be highly beneficial. In texture analysis, the most difficult problem is to define a set of meaningful features that include the texture characteristics. Several approaches exist for this problem including gray-level co-occurrence matrix (GLCM)[5], Fourier power spectrum[6], Gray Level Run Length Matrix, Gray Level Difference Statistics and so on[7]. Although these methods are useful in analysing natural tissues, they are not enough reliable to diagnose the suspected patients of bone marrow metastasis. Recently, multichannel analysis techniques have shown the high potential for texture description. The advantage of these techniques from the frequency-spatial viewpoint lies in the maximization of energy in both the region and frequency domain[8]. The use of the wavelet transform as a method of multichannel analysis was first proposed by Mallat[9]. Most of the previous studies have concentrated on the computer-aided diagnosis (CAD) of a tumor and lesion and different results have been obtained. Generally, the steps of these algorithms can be classified into two categories of feature extraction and samples classification. First, image features are extracted. These features usually include features of intensity (such as mean, variance, skewness, and kurtosis), texture features (such as energy, homogeneity, contrast, correlation) and shape measurements (such as area, perimeter, diameter, extent). For the feature extraction, different methods like wavelet transform, Shearlet transform, Curvelet transform, Fourier transform, Gabor filter, histogram, and statistical methods are proposed. The information acquired in this step is then passed to the samples classification step. For the feature classification and separation, a variety of approaches such as supervised and unsupervised artificial intelligence and methods such as the genetic algorithm, support vector machine, self-organizing maps, nearest neighbors, deep learning, decision trees, Bayes Nets, naive Bayes, Bayesian fuzzy clustering, logistic regression, and hybrid methods can be mentioned. Some of the recent studies on the feature extraction, classification and clustering have been shown in Table 1.

Table 1:. Summary of some studies on different methods of feature extraction, classification and clustering

Row	Author	Publication Year	multivariate Control Chart	Feature Extraction	Classification	Clustering	Method
1	El-Dahshan et al[10]	2010	——	√	——	——	Discrete Wavelet Transform(DWT)
2	Demirhan et al[11].	2011	——	√	——	——	Stationary Wavelet transform(SWT)
3	Ortiz et al[12].	2013	——	√	——	√	Histogram, Self-organizing maps(SOM), Neural networks
4	Rouhi et al[13].	2015	——	√	√	——	Cellular neural network(CNN),Genetic Algorithm(GA)
5	Rouhi et al[14].	2016	——	√	√	——	Artificial neural network(ANN),Memetic Algorithm(MA),naïve Bayes
6	Dora et al[15].	2017	——	√	√	——	Gabor filter, Particle Swarm Optimization(PSO),
7	Berbar[16].	2018	——	√	√	——	Gray level co-occurrence matrix (GLCM), Wavelet based contourlet, SVM
8	Öztürk et al[17].	2018	——	√	√	——	Gray level co-occurrence matrix (GLCM), Local Binary pattern (LBP), Gray Level Run Length Matrix (GLRLM), linear discriminant analysis (LDA)
9	Kriti et al[18].	2019	——	√	√	——	Fourier transform, SVM
10	Ayadi et al[19].	2019	——	√	√	——	2D-DWT, Bag-of-Words (BoW)
11	Al Ghayab et al[20].	2019	——	√	√	——	Tunable Q-factor wavelet transform (TQWT), Bagged trees (BT), K nearest neighbors (k-NN), (SVM)
12	Maharjan et al[21].	2019	——	——	√	——	Deep learning
13	Hashemzehi et al[22].	2020	——	——	√	——	Deep learning, CNN, NADE
14	Raja et al[23].	2020	——	√	——	√	Bayesian fuzzy clustering, Deep learning
15	Kaplan et al[24].	2020	——	√	√	——	local binary patterns (LBP), Knn, ANN, RF, LDA
16	Budak et al[25].	2020	——	√	√	——	Shearlet Transform ,GLCM, SVM
17	Siva Raja et al[26]	2020		√	√	√	Wavelet, deep autoencoder, Bayesian fuzzy clustering, regression
18	Biswas et al[27].	2020		√	√		contourlet and curvelet transform, SVM
19	**Proposed method**	2020		√	√	√	2DWT, Hotelling's T^2 multivariate control chart, Fuzzy c-Means

As shown in Table 1, in all of the mentioned methods, after the feature extraction, clustering or classification methods has been used for the diagnosis of patients suspected to cancer tumors, lesion or abnormal tissue. In this paper, for the first time, instead of classification and clustering methods, a

multivariate control chart with the Hotelling's T^2 statistic is used for the diagnosis of patients suspected to bone marrow metastasis. For this proposed, a control chart is designed for the bone marrow features of the metastasis suspected patients in Phase I. Then, using some patients samples, the performance of the control chart is evaluated, where the results show the validity of the proposed method. Since in each image the regions of interest are overlapping for the smallest and largest dimension of the mask, and because the fuzzy c-means (FCM) clustering algorithm is an overlapping clustering algorithm and one of the most popular clustering algorithms widely used in medical imaging, FCM clustering method is selected from the existing methods and is used as the comparison basis[28]. The validation results of the two methods revealed that the accuracy and specificity metrics are better for the multivariate Hotelling's T^2 control chart rather than FCM clustering method. The structure of this paper is as follows. In Section 2, the methodology is presented and explained step-by-step. The feature extraction results obtained from the proposed methodology along with the results obtained from the evaluation and validation studies are reported in Section 3. Finally, the conclusion and suggestions for future studies are included in Section 4.

Methods

The proposed methodology has been presented in Figure 1. Each step of this methodology is explained as follows:

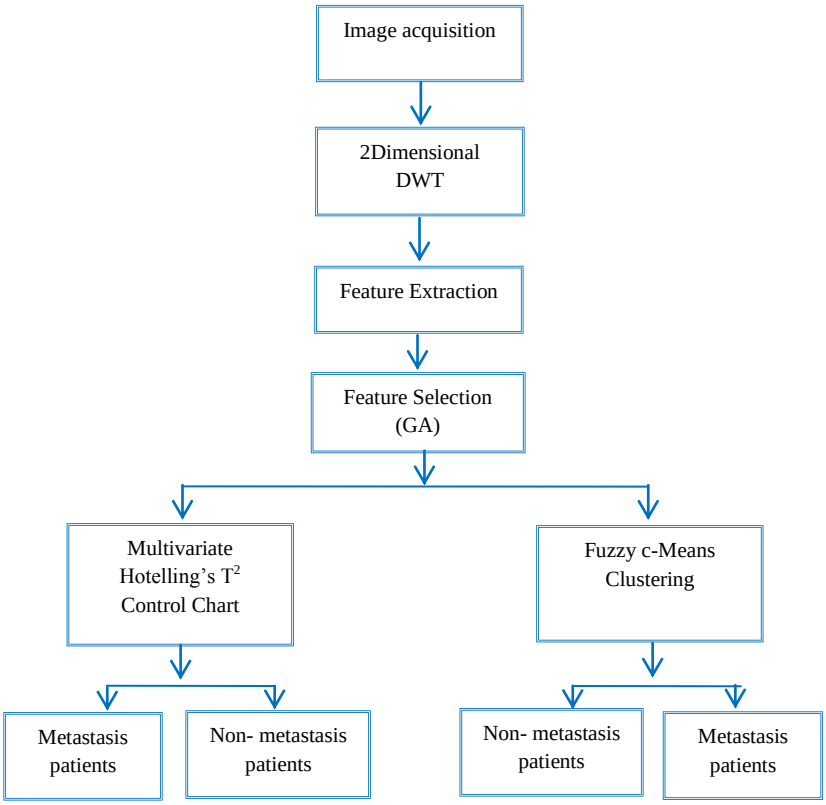

Figure 1: The schematic diagram of the proposed methodology

Image acquisition

The proposed techniques are applied on apparent diffusion coefficient (ADC) and T1-weighted type of MRI images with 256×256 resolution, DICOM (Digital imaging and communications in medicine) format and 16-bit mode for patients with breast cancer and

primary Tumor.

Two-dimensional discrete wavelet transform

Two-dimensional wavelet transform is widely used in image processing. There are two wavelet structures[29]: (1) pyramid-structured wavelet transform, in which a signal in lower frequency channels is decomposed into a set of frequency channels with narrower bandwidths. This transform is appropriate for signals whose suitable information exists in a low-frequency element. (2) Tree-structured wavelet transform that makes possible the decomposition of low, medium and high frequencies. In analyzing the bone marrow MRI of the pelvic region, low-frequency elements include information about general properties (shape) that are important clinically, and in the decomposition of higher frequency elements, there is information about textural details and region of interest, which are important for correct diagnosis. Therefore, decomposing all frequencies is helpful for this. Consequently, tree-structured wavelet analysis can include more beneficial information for this research. To obtain this transform, Mallat algorithm is used. Every time this algorithm is applied, the initial spectrum is transformed into two high- and low-frequency spectrums each with half the length of the initial spectrum. This procedure continues for the obtained low-frequency spectrum and the output is two other spectra each with one fourth the width of the initial spectrum. This procedure continues until a specified number of iterations is achieved (in this research, it was repeated one iteration). At last a spectrum is obtained that, in addition to preserving the structure of the initial spectrum, has fewer dimensions than it. The low-frequency spectrum is the approximation signal and the high-frequency spectrum is the detail signal[30]. The most common types of wavelet are continuous wavelet transform and discrete wavelet transform. A signal can be decomposed using two functions: scaling function ($\boldsymbol{\phi}_{j.k}$) and wavelet function ($\boldsymbol{\psi}_{j.k}$). Scaling functions decompose the image by making an approximation from the image (the general information of the image) and wavelet functions by calculating the difference between the information of two pixel neighborhoods (image details)[31].

$$\phi_{j.k}(x) = 2^{jl2}\phi\left(2^{j}x - k\right), \qquad (1)$$

$$\psi_{j.k}(x) = 2^{jl2}\psi\left(2^{j}x - k\right), \qquad (2)$$

where k is the location of the window on the x-axis and j is the scaling factor that identifies the window's width. It should be noted that this definition is for a one-dimensional wavelet transform. Since an image is defined as a two-dimensional signal, a two-dimensional wavelet transform must be used. Thus, in this study, the proposed method was developed based on the two-dimensional discrete wavelet transform. To do this, we applied a one-dimensional transform on the rows and columns of the image matrix so that by combining the elements of these two transforms, the two-dimensional transform is obtained. This process has been shown in Figure 2.

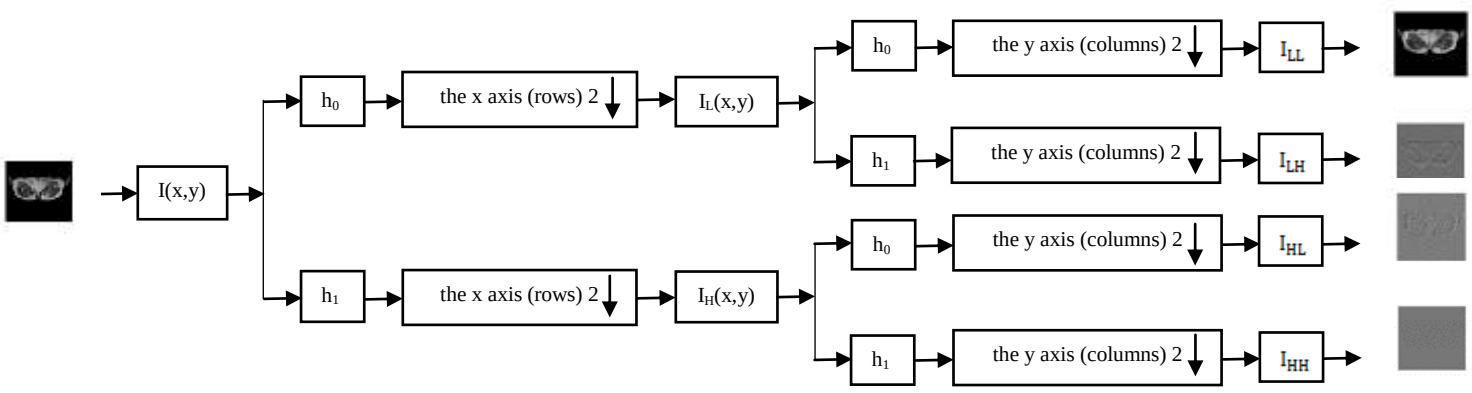

Figure 2:. The block diagram of the two-dimensional discrete wavelet transform

In this figure, the initial image along the x-axis (rows) passes through a low pass filter and a high pass filter and is down-sampled. This step results in two images, one of which includes the image's low frequencies $I_L(x, y)$ and the other includes the image's high frequencies $I_H(x, y)$. In the next step, each of these two images along the y-axis (columns) passes through a low pass filter and a high pass filter and is down-sampled. Therefore, four sub-images are obtained that are[32]: element I_{LL} corresponds to the image's low-frequency component along both directions that includes the image approximation. Element I_{LH} includes the horizontal details of the image. Element I_{HL} includes the vertical details of the image. Element I_{HH} includes the diagonal details of the image. Considering the wavelet's potentials in simultaneous extraction of time-frequency information for diagnosing lesion, using the MATLAB software, two wavelets have been applied: Haar wavelet as the base wavelet (mother wavelet) and Dmey wavelet for the segmentation of the lesion tissue. The reason for using these two wavelets is their better results than the other wavelet methods and their effective application[33,34]. The process of doing this can be described as follows: We apply a two-dimensional discrete wavelet transform with a Haar filter, which is the mother wavelet, on the whole image in two dimensions and obtain four output images. Then, from the bone marrow masks of the original image, we pick up a patch and this time we apply a two-dimensional wavelet on it using the Dmey filter. That is, in addition to the Haar filter previously applied on the whole image, again we separate a patch on which we apply a Dmey filter that generates four output images, from which the features are extracted in the next stage.

The feature extraction

If features are selected carefully, represent the maximum related information that the image provides for the complete characteristics of a lesion. The feature extraction methods analyze the images to extract the most considerable features. Considering the features description of the image, the extracted features must identify the characteristics of the desired lesion in the feature vector. The texture is an image feature that represents important information about the smoothness, regularity, roughness, and fineness of the surface and objects present in the image[31]. In recent years, texture analysis has had a key role in different applications especially for analyzing medical images. The features are used to identify and discriminate between the different textures of medical images. To extract the texture feature, four major methods are mentioned that are statistical methods, structural methods, model-based methods and transform methods[35,36]. In this research, some features of the image texture are extracted using the statistical methods and transform methods. For this, two feature categories are extracted from the image: one is energy and the other is the histogram of oriented gradients (HOG). The energy features are three types: horizontal energy, vertical energy, and energy of the image itself[37]. The second feature is the histogram of oriented gradients that are 16 types (which are explained in the following). First, each input image is transmitted into the wavelet space by applying a wavelet transform. Then, the energy and histogram of the oriented gradients of each image element are calculated by the following equations: the energy of an image is actually the representative of the image homogeneity and thus is an appropriate measure for estimating the image non-uniformity. The less the image uniformity, the less the energy would become. Therefore, the calculation of energy is defined as follows:

$$P(\mathrm{i}, \mathrm{j}) = \frac{h(i, j)}{NM}, \qquad \mathrm{i}=0, 1, \ldots, G-1, \quad \mathrm{j}=0, 1, \ldots, G-1 \qquad (3)$$

Angular second moment (Energy):

$$\sum_{i=0}^{G-1}\sum_{j=0}^{G-1}\left[p(\mathrm{i}, \mathrm{j})\right]^2, \qquad (4)$$

P (i, j): Probability density of occurrence of the intensity levels, h (i,j): value of intensity level histogram, MN: number of all image pixels, where M is the resolution at the

vertical axis and *N* is the resolution at the horizontal axis, *G*: total gray level of the image[38]. HOG was first introduced by Dalal[16] et al[39]. The histogram of oriented gradients has been based on the distribution of differential intensity histogram of an image[40]. It is used as an efficient method of describing texture types and deformable objects[41]. Moreover, it is helpful in medical imaging and has been considered as the best technique for diagnosing abnormal textures[42]. The gradient of an image is simply calculated by filtering the intensity data and by using two one-dimensional filters along the horizontal vector *x* and vertical vector *y* directions, [-1,0,1] and [-1,0,1]^T, described below[43]:

$$\nabla f(x,y) = \left(\frac{\partial f(x,y)}{\partial x}, \frac{\partial f(x,y)}{\partial y}\right), \quad (5)$$

$$\frac{\partial f(x,y)}{\partial x} = \frac{f(x+1,y) - f(x-1,y)}{(x+1)-(x-1)} \quad (6)$$

$$\frac{\partial f(x,y)}{\partial y} = \frac{f(x,y+1) - f(x,y-1)}{(y+1)-(y-1)}, \quad (7)$$

To define $G_x = \frac{\partial f(x,y)}{\partial x}$ and $G_y = \frac{\partial f(x,y)}{\partial y}$, the amplitude and orientation of each pixel is given as follows:

$$\left|\nabla f(x,y)\right| = \sqrt{G^2{}_x + G^2{}_y}, \quad (8)$$

$$\theta(x,y) = \tan^{-1}\left(\frac{G_y}{G_x}\right). \quad (9)$$

In this stage, after applying a two-dimensional wavelet transform on the whole image, a Dmey wavelet transform is used for texture analysis. For this aim, 76 features were extracted from the texture of the pelvic images to represent features of this region of interest. From each of the four images at the previous stage, 19 features were extracted. First, a two-dimensional gradient was calculated from the wavelet; once the energy of the gradient along the horizontal axis and then, the energy of the gradient along the vertical axis plus the energy of the wavelet image itself are calculated. Then, the angle between the horizontal and vertical gradients (from $-\pi$ to π divided into 16 parts). was calculated and a normalized histogram was constructed. That is, we computed the oriented gradient and then we obtained its histogram. Those 16 angles were considered as the histogram boundaries. Thus, we obtained 16 values of the normalized histogram with the probability of occurrence between 0 and 1. Finally, 19 (16 + 3) features were calculated one time for approximation sub-image channel I_{LL}, one time for horizontal sub-image channel I_{LH}, one time for vertical sub-image channel I_{HL}, one time for diagonal sub-image channel I_{HH}, and finally, 6 features were selected.

The feature selection

In all feature selection methods, it is tried to find a set of minimum features that contains the necessary and sufficient information for the desired purpose. The process of feature selection and removing unnecessary features has three basic steps: searching method, subset evaluation and a stop criterion[44]. The process of feature selection has been shown in Figure 3.

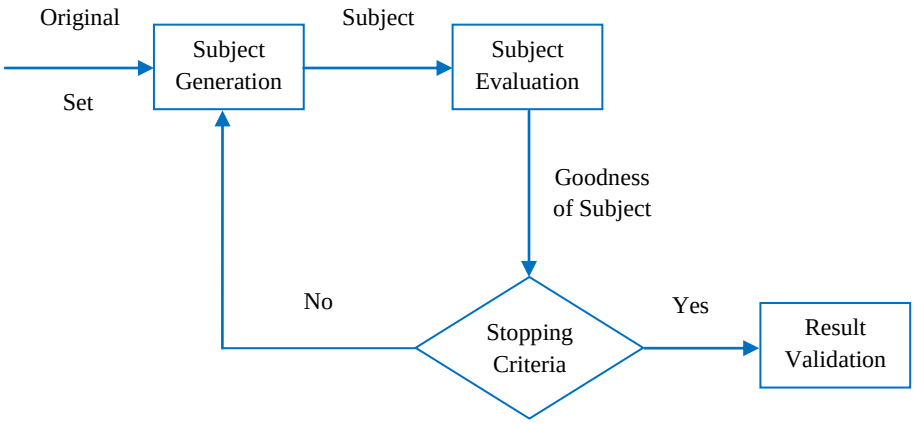

Figure 3: The feature selection process with validation

The methods of feature reduction are: 1- filter method (methods that get to the solution by using a set of formulas, such as Chi-square test and Euclidian distance), 2- wrapper method (methods that reach the solution by using an inference algorithm, like heuristic search algorithms), 3- embedded method (methods like decision tree that a set of operations is done by the algorithm itself and a set of features is selected)[45]. In this research, the final features are selected by applying the wrapper method and using the Genetic algorithm.

The Genetic Algorithm

Genetic algorithm is a type of evolutionary algorithms that uses the inheritance technique and mutation. This algorithm was initially introduced by John Henry Holland in 1967. In this algorithm, a population of candidate subsets is generated in each iteration, by applying the mutation and recombination operators on the elements of the previous population, new elements are generated. Using a fitness function, the fitness value of the current population's elements is obtained and the better elements are selected as the population of the next generation. In this method, finding the best solution is not guaranteed but relative to the time the algorithm is allowed to run, it always finds a good solution. exact methods can ensure optimal solutions for small-scale problems (n=30), but their computational time is large. In fact, the computational time of such methods grows exponentially with the increase of size and they almost give rise to computational error. On the contrary, the objective of applying GA on such problems is to evaluate its ability in obtaining optimal solutions and its convergence for different setups[46]. Besides, in GA, unlike exact algorithms, a set of solutions is produced at each iteration[47]. In short, this algorithm is appropriate for searching for the solution in large spaces. Regarding the above reasons and due to the largeness of this problem (204*176), we use GA instead of exact algorithms. The procedure of the algorithm is as follows:

1. A Genetic algorithm starts with an initial random population.

2. The algorithm generates a set of new populations (population and generations).in each iteration, it uses the individuals in the current generation to generate the next generation. To produce a new generation, the algorithm follows the following steps:

   - A score is dedicated to each member of the current population. This is done by calculating the fitness value of each individual present in the population.
   - The obtained fitness values are scaled to be in a more usable range of values.
   - Parents are selected regarding the fitness values dedicated to the individuals. Actually, the individuals with more fitness are used as parents.

- Children are generated using the parents. They are generated by applying random changes to one of the parents (mutation) and by combining the vectors of both parents (crossover) or by identifying elite children.

- The current population is replaced by the children and the next generation is formed.

3. The algorithm is stopped if one of the following stop criteria is met:

   - The number of generations: the algorithm is stopped when the number of generations reaches a certain number.

   - Time constraint: this constraint can be specified in terms of seconds.

   - Fitness constraint: the algorithm is stopped when the best fitness value among the current population is equal to or less than a certain value.

   - Stall generation: if there has been no improvement in a certain number of successive generations, the algorithm is stopped.

   - Stall time: if there has not been any improvement in the objective function in a certain time window, the algorithm is stopped [14].

This algorithm is implemented by the default toolbox of MATLAB. All parameters including the population, mutation, crossover and stop criterion have been the default values of the software. The cost function is to maximize the discrimination power of centers and minimizing the total number of the centers. since our GA is binary, we used zero and one numbers for the selection or not selection of the features. Since the chromosome length is considered as a 76-bit number, its zero bits indicate that the corresponding features are not selected in clustering and the ones represent the selected features. Thus, considering the cost function of minimizing error, the 76-bit chromosome, and zero and one denoting the selection and not selection of the features, six features are obtained. It should be noted that along with the error minimization, since the less number of features is desirable for us, we added the number of ones as the complementary or dual objectives to the main objective. Accordingly, the objective function was considered as the maximization of correctness and minimization of the selected features. The parameters of the GA algorithm is given as follows: Population size: 204, Chromosome length: 76, Type of genetic algorithm: Binary, Crossover percentage: 0.80, Mutation percentage: 0.1, Chromosome selection: Ideal method, Terminating condition: maximum iteration 700.

After implementing the GA, according to Figure 4, from the extracted features of the previous stage, six features are selected and feature vector is obtained and sent to the next stage for diagnosing of patients suspected to bone marrow metastasis. this paper uses wavelet transformation with a tree structure so that the decomposition of the low, medium, and high frequencies in the bone marrow MRIs of the pelvic region be possible. Applying the wavelet transformation to MRIs, the outputs will contain an approximated value including the basic characteristics of the image, details at the horizontal and vertical directions, in most cases include details like edges and high frequencies, and finally, diagonal details including low frequencies, mainly referred to image noise. In fact, the approximation coefficients represent low-pass filter output, including clinically important information about the shape of the bone marrow, and detail coefficients (horizontal, vertical, and diagonal details of the image) represent high-pass output, having information about the texture details and region of interest, which are important for the correct diagnosis. The four images observed in Figure 4 have been extracted in this manner.

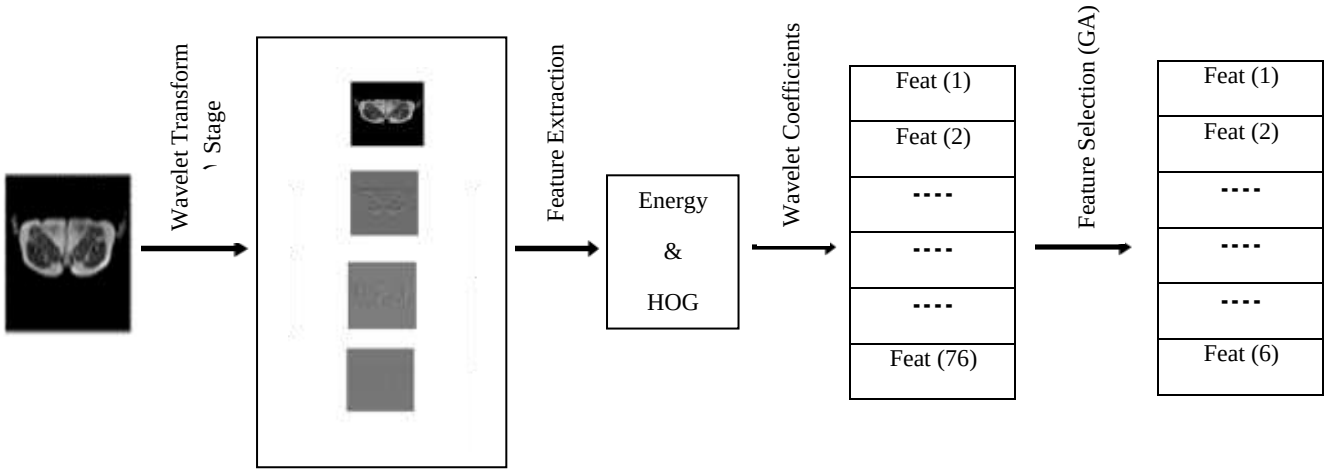

Figure 4 the schematic diagram for the extracted features and their reduction scheme (feature selection)

Clustering

Clustering means creating groups that are in a not categorized dataset and are of unsupervised type[48]. Clustering has two major parameters: inter-cluster distance and intra-cluster distance. To have an optimized clustering, the intra-cluster distance must be increased to its maximum and the inter-cluster distance must be decreased to its minimum[49]. Fuzzy c-Means clustering has many applications in different clustering problems. The purpose of this algorithm is to divide the data $\{X_1,\ldots, X_n\} \subset R_s$ into C clusters regarding the minimization of the minimum distance function:

$$J_m(U,V) = \sum_{k=1}^{n}\sum_{i=1}^{c} \mu^m{}_{ik} \left\| x_k - v_i \right\|^2, \qquad (10)$$

where m ($1 \le m \le \infty$) is the fuzziness parameter, $v_i \in R^s$ is the center of cluster i and $\mu_{ik} \in [0,1]$ is the membership degree of data to clusters. Using the optimization algorithm, the optimized values of $U=\{\mu_{ik}{}^m\}$ and $V=\{V_i, i=1,2,\ldots,c\}$ are obtained. In this formula (n_x and n_y are actually the number of rows and columns in the image matrix), n is the number of data points in the images.

then the new value of U (using the calculated value for V in the previous stage) is obtained using the following equation[50,51]:

$$\mu_{ik} = \sum_{j=1}^{c} \left(\frac{\left\| x_k - v_i \right\|}{\left\| x_k - v_j \right\|} \right)^{\frac{-2}{(m-1)}}, \qquad (11)$$

In this paper that all parameters have been based on the defaults of MATLAB software, by taking the maximum of the fuzzy memberships, which the FCM method in the software has calculated, we evaluate which cluster each of 76 features belongs to. For 2 to 6 clusters, the clustering does not yield appropriate solutions and the clusters are overlapping. However, for 7 clusters, it provides the best solution. With the try-and-error method, these 7 clusters have been selected with the goal of minimizing the errors and maximizing the correctness. The final result has been shown in Table 2.

Table 2. The final result of the clustering performed in MATLAB software

Center no. 1	Normal 43	Abnormal 0
Center no. 2	Normal 20	Abnormal 0
Center no. 3	Normal 33	Abnormal 0
Center no. 4	Normal 49	Abnormal 0
Center no. 5	Normal 0	Abnormal 7
Center no. 6	Normal 25	Abnormal 0
Center no. 7	Normal 27	Abnormal 0

based on Table 2, this paper differentiates two classes of bone marrows, metastasis bone marrows (Abnormal) and non-metastasis bone marrows (Normal), using seven-centers clustering. In fact, the centers of fuzzy clustering identify the center number of each cluster. Thus, each new input is assigned to one of these classes. As can be seen from the results, only center 5 belongs to metastasis (Abnormal) bone marrows and the others belong to non-metastasis (Normal) bone marrows. For example, in center 5, seven cases of metastasis bone marrows are observed, while it had no non-metastasis bone marrows. It should be noted that the clustering method has had no information about whether the patients have been metastasis or not (it has been totally blind), and this implies that the features of the metastasis and non-metastasis patients have been led to this results.

The multivariate Hotelling's T^2 control chart

Quality control problems in medical contexts may include more than one quality characteristic; that is, a vector of characteristics may exist. Especially, when these characteristics are dependent, an appropriate method must be provided for their simultaneous monitoring. Therefore, an extensive background has been established for multivariate statistical process control (MSPC). In this regard, two objectives must be satisfied: first, using a suitable control tool, the state of being in-control or not must be identified, and then, in case of being out-of-control, it must be possible to identify which ones of the quality characteristics have been the cause of variation[52]. As has been noted by Lowry and Montgomery[53], the most basic work in this area has been done by Hotelling, who proposed T^2 statistic and its distribution and used it in control charts. A multivariate control chart includes two phases: Phase I: analyzing a primary dataset which is supposed to be randomly selected from a process that is statistically in-control. Phase II: the control chart obtained in the previous phase is used for process control in the future. The most common statistics used in MSPC are Hotelling's T^2, MEWMA, and MCUSUM. Hotelling's T^2-statistic is used in two different contexts: one for individual observations and the other for grouped data, where the first is out of the scope of this research.

Based on what has been noted by Lowry and Montgomery[53], Mason and Young[54] and Bersimis[55]. the Hotelling's T^2 method incorporates the effects of all quality characteristics in a T^2 statistic and uses a χ^2 or F statistical distribution; if the parameters of the probability distribution function are known, χ^2 distribution is used, and otherwise, F distribution is used[53,56]. So in this research, second (F distribution) is used. If the process includes p quality characteristics, given the values of $\boldsymbol{\mu_0}$ and $\boldsymbol{\Sigma_0}$ (the parameters of the p-variate normal distribution), the value of the statistic used for the process is obtained as follows:

$$\chi^2_j = n\left(\overline{\mathbf{X}}_j - \boldsymbol{\mu}_0\right)^T \sum_0^{-1} \left(\overline{\mathbf{X}}_j - \boldsymbol{\mu}_0\right), \qquad (12)$$

where $\overline{\mathbf{X}}_j = \left(\overline{X}_{j1}, \overline{X}_{j2}, ..., \overline{X}_{jp}\right)^T$ and $\boldsymbol{\mu}_0 = \left(\mu_{01}, \mu_{02}, ..., \mu_{0p}\right)^T$. The upper control limit of this chart will be $UCL = \chi^2_{\alpha,p}$. If the parameters of the process are unknown and

estimated using the random samples, then F distribution is used. There are two phases for using the control chart. In phase one, when the multivariate process operates in a stable state, *m* initial *p*-variate random samples are selected and $\overline{\overline{\mathbf{X}}}$ and **S** statistics are calculated as estimates of **μ** and **Σ** parameters. The statistic used in this case is:

where

$$T^2_j = n\left(\overline{\mathbf{X}}_j - \overline{\overline{\mathbf{X}}}\right)^T \mathbf{S}^{-1}\left(\overline{\mathbf{X}}_j - \overline{\overline{\mathbf{X}}}\right), \qquad (13)$$

$$\overline{\overline{\mathbf{X}}} = \frac{1}{n}\sum_{j=1}^{n}\overline{\mathbf{X}}_j, \qquad (14)$$

$$\mathbf{S} = \frac{1}{n-1}\sum_{j=1}^{n}\left(\overline{\mathbf{X}}_j - \overline{\overline{\mathbf{X}}}\right)\left(\overline{\mathbf{X}}_j - \overline{\overline{\mathbf{X}}}\right)^T, \qquad (15)$$

In Phase I the upper control limit of the T^2 statistic is cacculated by using the following equation:

$$UCL = \frac{p(m-1)(n-1)}{mn-m-p+1} F_{a,p,mn-m-p+1} \qquad (16)$$

After computing the upper control limit of the T^2 statistic in Phase I, in the case that the process is stable we used this control limit in Phase II & the T^2 statistic in Equation[16]. In this paper, the normality test is first done for the 6 features extracted from the 197 samples of the previous stage. Since the normality is not confirmed, the samples are divided into groups of 5 samples. Again, the normality test is run, where all 6 features follows normal distribution. Then, using the Hotelling's T^2 control chart, the samples are evaluated and it is indicated that some samples are out-of-control. Thus, removing them, the above stages are repeated and it is indicated that the process is in-control and UCL=11.32 is obtained (Figure 5). Then, to become more assured and also evaluate the performance of the control chart, three metastasis patients samples are added to the chart. The chart is correctly identified them as metastasis patients and out-of-control samples (Figure 6).

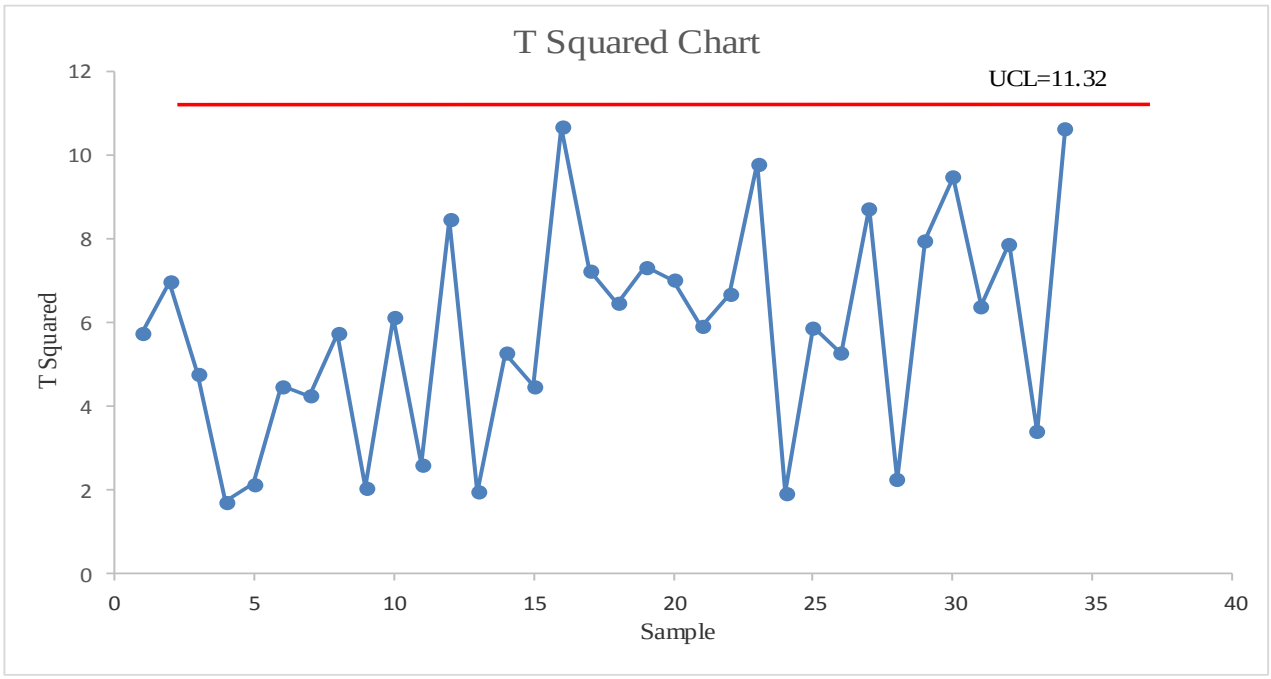

Figure 5: Multivariate Hotelling's T^2 control chart for the non-metastasis patient

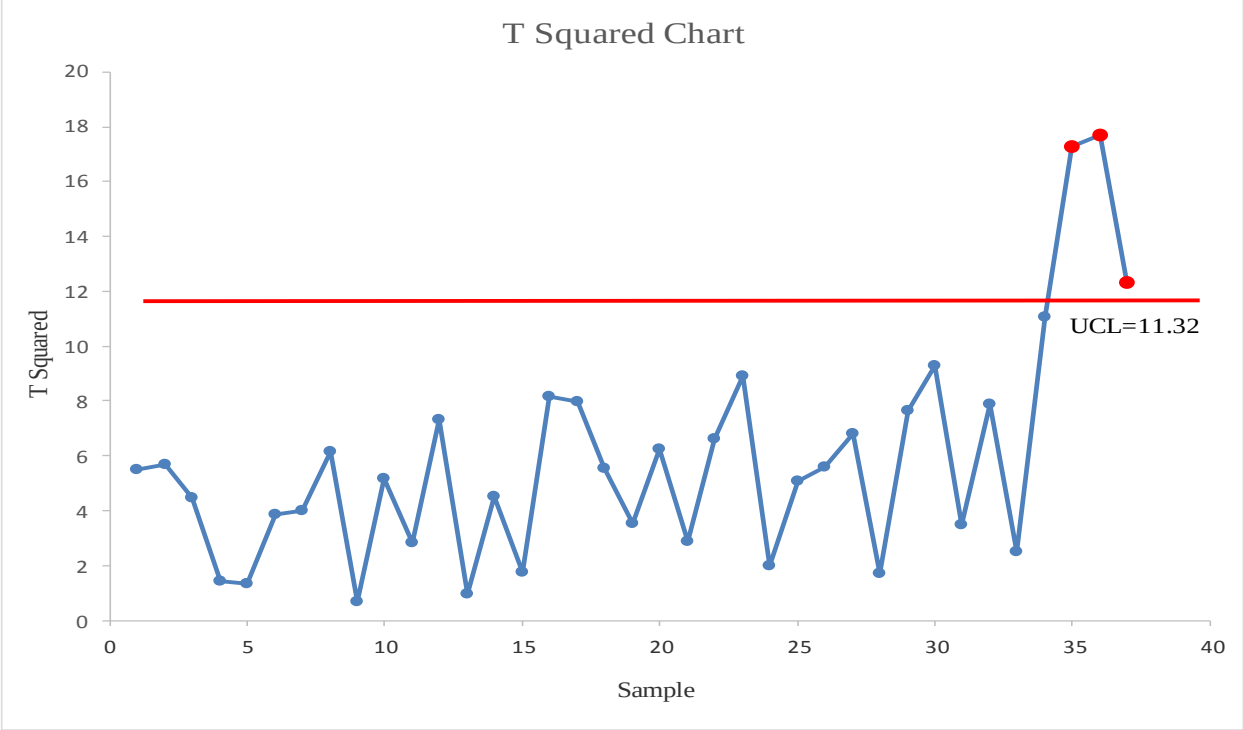

Figure 6: Multivariate Hotelling's T^2 control chart for the non-metastasis and metastasis patient

Results

In this paper, we used ADC and T1-weighted images of the pelvic region. For this aim, 204 bone marrow masks have been studied. The images were 256×256 pixels and contained 65536 grey levels. The regions of interest (bone marrows) in the image have selected by overlapping masks (with the smallest and largest dimensions of 10×10 pixels and 105×80 pixels). The region of interest is selected such that it includes only the bone marrow. In Figure 7, an example of the used images is shown. In the first stage, after applying the two-dimensional discrete wavelet transform (including Harr and Dmey wavelets) to the images, the features are extracted. In the second stage, using the GA, out of the extracted features, we extracted 6 features. In the third stage, using the fuzzy clustering algorithm and multivariate Hotelling's T^2 control chart, metastasis patients are identified. The two methods are compared to each other and the more accuracy and specificity of the multivariate Hotelling's T^2 control chart are shown (Table 3). To validate the diagnosis results, we used sensitivity, specificity and accuracy measures, which are defined as follows [14]:

$$Specificity = \frac{TN}{TN + FP}, \qquad (17)$$

$$Sensitivity = \frac{TP}{TP + FN}, \qquad (18)$$

$$Accuracy = \frac{TP + TN}{TP + TN + FN + FP}. \qquad (19)$$

Accuracy denotes the ratio of patients who were correctly diagnosed to the total number of patients. Sensitivity denotes the correct diagnosis of the metastasis patients using the control chart. Specificity refers to the ratio of patients who are non- metastasis using the control chart.

TP: number of metastasis patients correctly diagnosed positive.

TN: number of ones who are not metastasis patients and correctly diagnosed.

FP: number of ones who are not metastasis and wrongly diagnosed.

FN: number of metastasis who are wrongly diagnosed.

Table 3: The comparison of the proposed methods in terms of specificity, sensitivity, accuracy (in percent)

Proposed method	Specificity(%)	Sensitivity(%)	Accuracy(%)
Hotelling's T^2	100	100	100
FCM	97.14	100	97.37

As mentioned, Fig. 7 is an example of the images used in this study, where in the red regions (masks) indicate pelvic bone marrows in T1weighted magnetic resonance images. After the feature extraction by the proposed methods from pelvic bone marrows, it was identified that left image masks belong to non-metastasis bone marrows and right image masks belong to metastasis bone marrows.

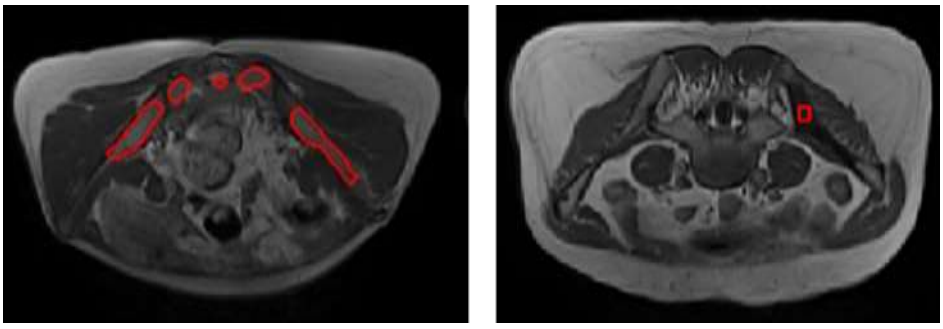

Figure 7: a-left) Image T1-weighted of bone marrow of the pelvic region of a non-metastasis patient, b-right) Image T1-weighted of an individual with breast cancer with bone marrow metastasis in pelvic region

Discussion

In this paper, using multivariate control charts, we proposed an efficient method for diagnosing bone marrow metastasis in the pelvic region, with a primary breast tumor, in MRI images. For this, using a two-dimensional discrete wavelet transformation, we extracted energy and histogram of oriented gradients features of the ADC and T1 images from the patients suspected to bone marrow metastasis. To demonstrate the diagnosis accuracy of the proposed method, we compared it to some methods of the literature. The results confirmed the superiority of the proposed method, and thus, it can help doctors in diagnosing and interpreting medical data, especially those of cancer patients.

onclusion and a suggestion for future research

Regarding the importance of refractory disease in healthcare, diagnosing bone marrow metastasis in medical images, with high accuracy such that it can be used as a support system or a doctor's assistant, is vital. In this paper, to achieve this goal, some features of medical images were extracted using a two-dimensional discrete wavelet transform. Then, for data dimension reduction and features selection, a genetic algorithm was used. After that, using a fuzzy c-Means clustering method and a multivariate Hotelling's T^2 control chart, bone marrow metastasis patients are

diagnosed. Finally, the proposed two methods were compared and the results showed that the accuracy and specificity measures are higher for the multivariate Hotelling's T^2 control chart than those for the other method. Magnetic resonance imaging (MRI) is an effective tool in diagnosis, treatment design, and also in the cancer treatment process. In this research, we only worked on the diagnosis subject. The other two subjects can be considered by researchers. The other features than those were extracted in this research can be utilized in image analysis and comparison can be made with the methods of this research. In this research, MRI images of the pelvis have been used, while the whole-body magnetic resonance imaging (WB-MRI) can be used even to identify the location of the lesion (tumor and metastasis). Developing a multivariate fuzzy control chart rather than the multivariate Hotelling's T^2 control chart can be a fruitful area for future research.

Competing interest:

The authors declare no competing interest

Authors contributions:

The Author have the same contributions in this study.

References:

1. Moulopoulos L.A., Assilis Koutoulidis V. Bone Marrow MRI, Springer Milan, 2015.

2. Mohandas N., Evans E. Mechanical properties of the red cell membrane in relation to molecular structure and genetic defects. Annual review of biophysics and biomolecular structure, 1994; 23(1): 787-818.

3. Crow P., Stone N., Kendall CA., Persad RA., Wright M.P.J. Optical diagnostics in urology: current applications and future prospects. BJU International, 2003; 92(4): 400-407.

4. Beutel J., Kundel H.L., Van Metter R.L. Handbook of medical imaging: physics and psychophysics vol.1: Spie Press. 2000.

5. Haralick R.M., Shanmugam K., Dinstein I. Texture features for image classification, IEEE Transactions on Systems, Man and Cybernetics, 1973; 6(3): 610-621.

6. Lendaris G.G., Stanley G.L. Diffraction pattern sampling for automatic pattern recognition, Proceedings of the IEEE, 1970; 58(2): 198-216.

7. Weszka J.S., Dyer C.R., Rosenfeld A. A comparative study of texture measures for terrain classification, IEEE Transactions on Systems, Man and Cybernetics, 1976; 6(4): 269-285.

8. Bovik AC., Clark M., Geisler WS. Multichannel texture analysis using localized spatial filters, IEEE Transactions on Pattern Analysis and Machine Intelligence (PAMI), 1990; 12(1): 55-73.

9. Mallat S. A theory for multi resolution signal decomposition: the wavelet representation, IEEE Transactions on Pattern Analysis and Machine Intelligence, 1989; 2(7): 674-693.

10. El-Dahshan E.A., Hosny T., M.Salem A.B. Hybrid intelligent techniques for MRI brain images classification, Digital Signal Processing, 2010; 20(1): 433–441.

11. Demirhan A., Guler I. Combining stationary wavelet transform and self-organizing maps for brain MR image segmentation, Engineering Applications of Artificial Intelligence, 2011; 24(2): 358–367.

12. Ortiz A., Górriz J.M., Ramírez J., Salas-González D., Llamas-Elvira J.M. Two fully-unsupervised methods for MR brain image segmentation using SOM-based strategie, Applied Soft Computing, 2013; 13(5): 2668–2682.

13. Rouhi R., Jafari M., Kasaei S., Keshavarzian P. Benign and malignant

breast tumors classification based on region growing and CNN segmentation, Expert Systems with Applications, 2015; 42(3): 990-1002.

14. Rouhi R., Jafari M. Classification of benign and malignant breast tumors based on hybrid level set segmentation, Expert Systems with Applications, 2016; 46(C): 45–59.

15. Dora L., Agrawal S., Panda R., Abraham A. An evolutionary single Gabor kernel based filter approach to face recognition, Engineering Applications of Artificial Intelligence, 2017; 62 (C): 286–301.

16. Berbar M.A. Hybrid methods for feature extraction for breast masses classification, Egyptian Informatics Journal, 2018; 19(1): 63-73.

17. Ozturk S., Akdemir B. Application of feature extraction and classification methods for histopathological image using GLCM, LBP, LBGLCM, GLRLM and SFTA, Procedia Computer Science, 2018; 132(1): 40–46.

18. Kriti, V.J. and Agarwal, R. Effect of despeckle filtering on classification of breast tumors using ultrasound images, Biocybernetics and Biomedical Engineering, 2019; 19(2): 536-560.

19. Ayadi A., Elhamzi W., Charf I., Atri M. A hybrid feature extraction approach for brain MRI classification based on Bag-of-words, Biomedical Signal Processing and Control, 2019; 48(1): 144–152.

20. Al Ghayab H.R., Li Y., Siuly S., Abdulla S. A feature extraction technique based on tunable Q-factor wavelet transform for brain signal classification, Journal of Neuroscience Methods, 2019; 312(1): 43–52.

21. Maharjan, S., Alsadoon, A., Prasad P.W.C. and Alsadoon, O.H. A novel enhanced softmax loss function for brain tumour detection using deep learning, Published online in Journal of Neuroscience Methods, 2019; doi: 10.1016/j.jneumeth.2019.108520.

22. Hashemzehi R., Mahdavi, S.J., Kheirabadi, M., Kamel, S.R. Detection of brain tumors from MRI images base on deep learning using hybrid model CNN and NADE, Published online in Biocybernetics and Biomedical Engineering, 2020, doi: 10.1016/j.bbe.2020.06.001.

23. Raja, S., P.M., Rani and Viswasa, A. Brain tumor classification using a hybrid deep autoencoder with bayesian fuzzy clustering-based segmentation approach, Biocybernetics and Biomedical Engineering, 2020; 40(1) : 440-453.

24. Kaplan k., Kaya, Y., Kuncan, M. and Ertunc, H.M. Brain tumor classification using modified local binary patterns (LBP) feature extraction methods, Published online in Medical Hypotheses, 2020; doi: 10.1016/j.mehy.2020.109696.

25. Budak, U., Guzel, A.B. Automatic grading system for diagnosis of breast cancer exploiting co-occurrence shearlet transform and histogram features, Innovation and Research in BioMedical engineering, 2020; 41(2): 106-114.

26. Siva Raja, P.M., Viswasa rani, A. Brain tumor classification using a hybrid deep autoencoder with Bayesian fuzzy clustering-based segmentation approach, Bio cybernetics and Biomedical Engineering, 2020; 40(1): 440-453.

27. Biswas, S., Sil, J. An efficient face recognition method using contourlet and curvelet transform, Journal of King Saud University - Computer and Information Sciences, 2020; 32(6): 718-729.

28. Li B.N., Chui C.K., Chang S., Ong S.H. Integrating spatial fuzzy clustering with level set methods for automated medical image segmentation, Computers in Biology and Medicine, 2011; 41(1): 1–10.

29. Garnavi R., Aldeen M., Bailey J. Classification of melanoma lesions using wavelet-based texture analysis, IEEE International Conference on Digital Image Computing: Techniques and applications, Sydney, NSW, Australia, 2010.

30. Beylkin G., Coifman R., Rokhlin V. Fast wavelet transforms and numerical algorithms I, Communications on PURE AND APPLIED MATHEMATICS, 1991; 44(2): 141-183.

31. Gonzalez R.C., Woods R.E. Digital image processing 3rd edition. Prentice Hall, 2007.

32. Sidney Burrus C., Gopinath R.A. Introduction to wavelets & wavelet transforms, Prentice Hall, New Jersey,1998.

33. Majak J., Pohlak M., Karjust K., Eerme M., Kurnitski J., Shvartsman B.S. New higher order haar wavelet method: Application to FGM structures, Composite Structures, 2018; 201(1): 72-78.

34. Wu M.T. Wavelet transform based on meyer algorithm for image edge and blocking artifact reduction, Information Sciences, 2019; 474(1): 125–135.

35. Tuceryan M., Jain A.K. Handbook of pattern recognition & computer vision pages, 1993; 235-276.

36. Castellano G., Bonilha L., Li L.M., Cendes F. Texture analysis of medical images, Clinical Radiology, 2004; 59(12): 1061–1069.

37. Walvick R.P., Patel K., Patwardhan S.V., Dhawan A.P. Classification of melanoma using wavelet-transform-based optimal feature set. Medical Imaging: Image processing, 2004; 5370(1): 944-952.

38. Ain Q., Arfan Jaffar M., Choi T. Fuzzy anisotropic diffusion based segmentation and texture based ensemble classification of brain tumor, Applied Soft Computing, 2014; 21(1): 330–340.

39. Dalal N., Triggs B. Histograms of oriented gradients for human detection, In International Conference on Computer Vision & Pattern Recognition San Diego, United States (CVPR), 2005; 886-893.

40. Xu Y., Imou K., Kaizu Y., Saga K. Two-stage approach for detecting slightly overlapping strawberries using HOG descriptor, Biosystems Engineering, 2013; 115(2): 144–153.

41. Felzenszwalb P.F., Girshick R.B., McAllester D., Ramanan D. Object detection with discriminatively trained part-based models, IEEE Transactions on Pattern Analysis and Machine Intelligence, 2010; 32(9): 1627–1645.

42. Song L., Liu X., Ma L., Zhou C., Zhao X., Zhao Y. Using HOG-LBP features and MMP learning to recognize imaging signs of lung lesions, in: Proceedings of the 25th International Symposium on Computer-Based Medical Systems (CBMS), 2012: 1–4.

43. Ergin S., Kilic O. A new feature extraction framework based on wavelets for breast cancer diagnosis, Computers in Biology and Medicine, 2014; 51(1): 171–182.

44. Nong Y. The handbook of data mining. Lawrence erlbaum associates, Publishers Mahwah, New Jersey London, 2003.

45. Chandrashekar G., Sahin F. A survey on feature selection methods, Computers and Electrical Engineering, 2014; 40(1): 16–28.

46. Singhi, S.K., Liu, H. Feature subset selection bias for classification learning, Appearing in Proceedings of the 23rd International Conference on Machine Learning, Pittsburgh, PA, 2006; 849–856

47. Yang, J., Honavar, V. Feature subset selection using a genetic algorithm, IEEE Intelligent Systems, 1998; 13(2): 44-49.

48. Chuang K., Tzeng H. , Chen S., Wu J., Chen T. Fuzzy c-means clustering with

spatial information for image segmentation, Computerized Medical Imaging and Graphics, 2006; 30(1): 9-15.

49. Haykin S. N. Network, A comprehensive foundation, Neural Networks, 2004.

50. Prabha S., Sujatha C.M. Proposal of index to estimate breast similarities in thermo grams using fuzzy C means and anisotropic diffusion filter based fuzzy C means clustering, Infrared Physics and Technology, 2018; 93(1): 316–325.

51. Hathaway R.J, Bezdek J.C, Hu Y. Generalized fuzzy c-Means clustering strategies using Lp norm distances, IEEE Transactions on Fuzzy Systems, 2000; 8(5): 576 – 582.

52. Sogandi, F., Aminnayeri, M. The effect of estimation error on risk-adjusted bernoulli GEWMA control chart in multistage healthcare processes. International Journal of Hospital Research, 2019; 8(1): 1-18.

53. Lowry C.A., Montgomery D.C. A review of multivariate control charts, IIE Transactions, 1995; 27(6): 800-810.

54. Mason, R.L., Young, J.C. Implementing multivariate statistical process control using hotelling's T^2 statistic, Quality Progress, 2001; 34(1): 71-73.

55. Bersimis S., Panaretos J. Psarakis S. Multivariate statistical process control charts and the problem of interpretation: A short overview and some applications in industry, 7th Hellenic European Conference on Computer Mathematics and its Applications, Athens Greece, 2005: 1-6.

56. Chong, N.L., Khoo, M.B.C. Hotelling's T^2 control charts with fixed and variable sample sizes for monitoring short production runs, Quality and Reliability Engineering International, 2019; 35(1): 14–29.

Please cite this article as:

Mahmood Shahrabi, Amirhossein Amiri, Hamidreza Saligheh Rad, Sedigheh Ghofrani .The Diagnosis of Patients Suspected to Bone Marrow Metastasis based on Multivariate Control Chart.. Int J Hosp Res. 2020;9 (2).